sustainability

MDPI

Article

Experimental Study on the Performance Decay of Permeable Asphalt Mixture in Seasonally Frozen Regions under Freeze-Thaw Cycles

Chao Chai, Yong-Chun Cheng, Yuwei Zhang *, Yu Chen and Bing Zhu

College of Transportation, Jilin University, Changchun 130025, China; chaichao18@mails.jlu.edu.cn (C.C.); chengyc@jlu.edu.cn (Y.-C.C.); jtxycyjlu@163.com (Y.C.); zhubing18@mails.jlu.edu.cn (B.Z.)

* Correspondence: ywzhang@jlu.edu.cn; Tel.: +86-0431-850-94771

Received: 16 March 2020; Accepted: 5 April 2020; Published: 8 April 2020

Abstract: This paper focuses on the freeze-thaw cycles (F-T cycles) resistance of porous asphalt mixture (PAM) with different air voids in order to explore the gradation of the PAM suitable for seasonal freezing regions. Three sets of PAMs with 18%, 21%, and 25% air voids were designed. After 0–20 F-T cycles, the effects of F-T cycles on the performance degradation of three groups of PAMs were studied by performing a low-temperature splitting test with acoustic emission technology, a normal temperature splitting test, a compression test, a Cantabro particle loss test, and a dynamic creep test. The results show that the damage process of PAM caused by multiple F-T cycles could be more clearly defined by acoustic emission parameters. In addition, the larger the air void, the smaller its indirect tensile strength and compression strength, and the worse its particle loss resistance and high-temperature stability, which made the adverse effect of F-T cycles more significant. Therefore, the air void of PAM used in seasonal freezing regions is suggested to be less than 21%.

Keywords: eco-friendly pavement; porous asphalt mixture; freeze-thaw cycles; air voids

1. Introduction

Green, ecological, and sustainable development methods are gradually being respected by people all over the world [1–3]. In the field of pavement engineering, functional pavement has been widely studied in recent years [4–6], and permeable asphalt pavement has become the focus of scholars. Permeable asphalt pavement has a large void structure, which can improve the safety of driving on rainy days, accelerate the natural water cycle, and reduce the adverse impact of road engineering on the natural environment. At the same time, it can reduce driving noise and improve driving comfort. Permeable pavement is more sustainable compared with traditional dense pavement. Therefore, the preparation technology and performance evaluation of permeable asphalt have become the focus of scholars all over the world.

Tang [7] applied a finite element model to analyze the skid resistance of vehicles under different precipitation intensities and considering the pavement's geometric design, tire tread design, and tire operating conditions. The results showed that under heavy rainfall conditions, skid resistance decreases rapidly with increasing vehicle speed. Therefore, the application of porous asphalt mixture (PAM) is conducive to driving safety in rainy weather. Liu et al. [8] studied the effect of different grades of porous ultra-thin overlay on skid resistance. The results showed that coarse-graded porous ultra-thin overlay is more conducive to improving the skid resistance of pavement. Khaki et al. [9] compared the noise reduction performance of porous asphalt pavement and densely graded pavement. It was found that PAM has better noise reduction performance, and the application of PAM can effectively reduce noise pollution. Although a large number of studies have shown the superiority of PAM, few studies have been conducted on the applicability of PAM in seasonal freezing regions.

In China, with the vigorous implementation of road construction, natural aggregate resources are exploited, and the problems caused by aggregate shortages become more and more prominent [10,11]. Therefore, how to use industrial wastes (steel slag, fly ash, waste oil shale, and so on) for pavement materials has become a research hotspot. Zarrinkamar et al. [12] studied the effects of coal combustion ash (CCA) and lime-activated coal waste ash (LA-CWA) on the performance of cold recycled asphalt pavement on-site. According to the results, CCA can replace cement as a stabilizer for asphalt pavement. Yan et al. [13] discussed the effect of municipal solid waste incineration (MSWI) fly ash on the properties of asphalt mortar. The results of a series of viscoelastic experiments showed that the addition of MSWI significantly improves the high-temperature performance of asphalt, and can reduce energy consumption and environmental pollution. Cheng et al. [14] studied the effect of recycling waste oil shale on the performance of asphalt pavement. The results showed that the addition of oil shale can significantly improve high-temperature stability and also enable sufficient low-temperature performance. Liu et al. [15] studied the properties of PAM with steel slag as aggregate and the experiments showed that it has good permeability, water stability, and high-temperature stability. The above research shows that the use of some industrial waste residues in road construction can save resources and reduce the extraction of natural resources.

Northeast of China is a typical seasonal frozen region. For example, it is hot and rainy in summer in Changchun city, Jilin province, and the daily average maximum temperature in June and July can reach 28 and 29 °C respectively. However, it is cold and dry in winter, and the daily average minimum temperature in December and January can reach −16 and −19 °C respectively. In the context of global climate change, Changchun city experienced continuous heavy rain in the summer of 2017–2019, which led to urban flooding. This brings serious inconvenience to the normal operation of transportation, and even threatens the safety of pedestrians. Therefore, it is necessary and urgent to use permeable pavement in this area. In addition, during the transition between winter and spring, the pavement structure in the northeast of China is often subjected to the effects of freeze-thaw cycles (F-T cycles) due to the large temperature difference between day and night [16–18]. Some studies have shown that the freeze-thaw cycle is an important factor affecting the long-term performance of asphalt mixture [19–21]. Furthermore, it has been shown that air voids have a great influence on the freeze-thaw resistance of asphalt mixture [22–24]. However, in the technical specifications for permeable asphalt pavement (CJJ/T 190-2012) [25], only the general range of air voids of PAM is specified. For northeast regions of China with special climatic conditions, how to determine the appropriate gradation of PAM is an urgent problem. So far, few such studies have been published.

Therefore, based on the previous research of the research group [26,27], the following tests have been carried out for this paper: with steel slag as aggregate, three groups of PAMs with air voids of 18%, 21%, and 25% were designed and manufactured. The F-T cycles of three groups of mixtures were carried out 0–20 times in a laboratory using a low-temperature tank and constant-temperature water tank. After corresponding F-T cycles, three groups of PAMs were subjected to a low-temperature splitting test, a normal temperature indirect tensile and compression test, a Cantabro particle loss test, and a dynamic creep test. The purpose was to study the effect of F-T cycles on three groups of PAMs with different air voids through the above tests, and to study the PAMs suitable for seasonal freezing regions from the perspective of frost resistance.

2. Materials and Methods

2.1. Materials and Gradation Design

The coarse and fine aggregates used in this study were steel slag, produced in Jilin City, Jilin Province. The binder used was SBS (styrene-butadiene-styrene) modified asphalt, in which the SBS content was 4%, and it was produced in Liaoning Province. In addition, in order to increase the viscosity of the binder, a 10% waste rubber powder was added to the PAM using a dry process, and it was produced in Jilin Province. The filler used in this study was limestone powder, which is also

produced in Jilin Province. The specific performance indicators of all materials refer to a previous study [27].

In this study, three kinds of PAM gradation were designed. According to the technical specifications for permeable asphalt pavement (CJJ/T 190–2012) [25], the upper limit, median gradation, and lower limit were selected. Their air voids were 18%, 21%, and 25%, respectively, and they are expressed as PAM-18, PAM-21, and PAM-25. The gradation curve is shown in Figure 1.

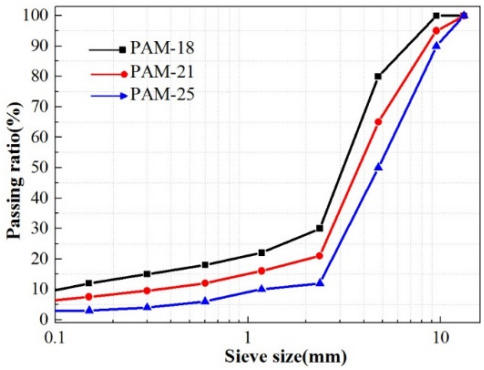

Figure 1. Gradation curves of three porous asphalt mixtures (PAMs).

2.2. Experimental Methods

2.2.1. Freeze-Thaw Cycle

Three groups of Marshall specimens with air voids of 18%, 21%, and 25% were prepared with reference to the standard test methods of bitumen and bituminous mixtures for highway engineering (JTG E20-2011) [28]. Each group had 75 specimens in total. Then, each group of specimens was subjected to 0, 5, 10, 15, 20 F-T cycles respectively. Each time before a test piece was frozen, it was sealed separately with a plastic bag, and then 15ml of water was poured into the bag. Then we immediately put the test piece into the refrigerator. Each freeze-thaw cycle included freezing the test piece in a −18 °C refrigerator for 16 h and then thawing it in 25 °C water for 8 h.

2.2.2. Low-Temperature Splitting Test

A low-temperature splitting test was used to characterize the changing low-temperature performance of PAM with different air void under F-T cycles. In order to further understand the damage effects of F-T cycles on specimens, acoustic emission technology was also used during the splitting test. Acoustic emission technology, as a damage detection technology, has been gradually applied to the field of asphalt mixtures in recent years [29,30]. During the experiment, the surface of the acoustic emission sensor was evenly coated with coupling agent, and then the sensor was clamped on the surface of a test piece with a rubber band. Subsequently, during the whole loading stage, the energy released by a specimen during the destruction process was measured by the sensor in the form of acoustic energy. Then it was transmitted to the computer through the signal amplifier. Finally, the influence of the low-temperature performance of PAM was further investigated through the analysis of the relevant parameters. Figure 2 shows the low-temperature splitting test set-up.

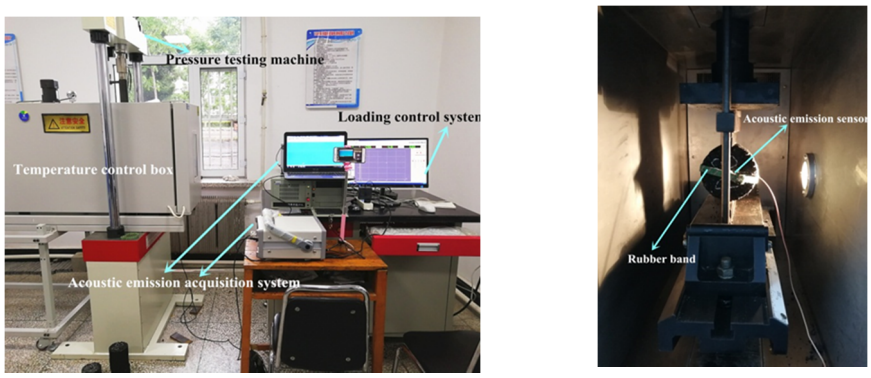

(**a**) General diagram of the test site (**b**) Inside the temperature control box

Figure 2. The low-temperature splitting test set-up.

2.2.3. Indirect Tensile and Compression Test at Room Temperature

The two tests were performed using an electro-hydraulic servo material testing machine. The experimental temperature was 25 °C. Before the tests, the specimens were kept in the incubator for 5 h; the loading rate was 1 mm/min. Both test results are expressed in terms of strength and failure strain. According to T 0716-2011 and T 0713-2000 in the specifications [28], the calculation methods are shown in Equations (1)–(4).

$$R_T = 0.006287 P_T / h \tag{1}$$

$$\varepsilon_T = X_T(0.0307 + 0.0936\mu)/(1.35 + 5\mu) \tag{2}$$

where R_T is indirect tensile strength, P_T is maximum force in the indirect tensile test, h is the height of specimen, X_T is the deformation in the horizontal direction, and ε_T is the indirect tensile failure strain.

$$R_c = 4P/\pi d^2 \tag{3}$$

$$\varepsilon_l = \Delta l / l \tag{4}$$

where R_c is compressive strength, P is maximum force in the compression test, d is the diameter of specimen, Δl is the deformation in the compressive test, and ε_l is the compressive failure strain.

2.2.4. Cantabro Particle Loss Test

The Cantabro particle loss test was used to characterize the effects of F-T cycles on the spalling resistance of PAMs with different air voids. Before the test, all the test pieces were placed in a 20 °C constant-temperature water tank for 20 h. Then we took out a test piece immediately, wiped off the surface water gently, and marked the mass of the test piece as m_0. The test piece was then placed in a Los Angeles testing machine and rotated 300 revolutions. After the machine stopped, we weighed the residual mass of the test piece as m_1, and the Cantabro particle loss rate was calculated by Equation (5).

$$\Delta m = (m_1 - m_0)/m_0 \times 100\% \tag{5}$$

2.2.5. Dynamic Creep Test

According to the method in BS EN 12697-25 [31], the dynamic creep test was used to characterize the effect of F-T cycles on the high-temperature performance of three PAMs. A servo pneumatic multifunctional testing machine was used in the test (NU-14, Cooper Technologies Ltd, UK). All the test pieces were kept in a 50 °C temperature box for 5 h. In addition, before the test started, a preload of 15 kPa was applied to the test piece for 30 s to ensure that the tester indenter and the test piece were tightly combined. The test loading frequency was 0.5 Hz, first loading for 1 s and then unloading for 1 s. One cycle was 2 s and the load was 300 kPa. The total test time was 3600 s. Figure 3 shows

the test site. Creep strain slope and creep modulus were used to characterize the high-temperature performance of three PAMs. The two parameters were calculated by the Equations (6) and (7):

$$f_c = (\varepsilon_{n1} - \varepsilon_{n2})/(n_1 - n_2) \times 1000 \quad (6)$$

$$E_n = \sigma/10\varepsilon_n \quad (7)$$

where f_c is the creep strain slope, and ε_{n1}, ε_{n2} are the cumulative axial strain of the specimen after n_1, n_2 loading cycles, n_1 is 1800, and n_2 is 400. E_n is the creep modulus, σ is applied stress, and ε_n is the cumulative axial strain of the specimen after 1800 loading cycles.

(**a**) General diagram of the test site (**b**) The test piece in creep test

Figure 3. Dynamic creep test set-up.

3. Results and Discussion

3.1. Low-Temperature Splitting Test

As shown in Figure 4, in order to analyze the damage effects of F-T cycles on three groups of PAMs from the perspective of acoustic emission parameters, the load time-load curve, energy value curve was obtained by analyzing the collected acoustic emission data. The energy value is a typical parameter in acoustic emission phenomenon. The larger the energy value, the greater the energy released by the specimen under load; that is, the more obvious the damage. Specifically, first, the entire loading process was divided into three stages by the intensity of the energy values. The first stage: no acoustic emission signal was generated during the loading process. It is shown that the test piece did not suffer damage at this stage. Only deformation occurred, no energy was released. The second stage: the acoustic emission signal began to appear intermittently. At this stage, the energy value of the acoustic emission signal was relatively small. This indicates that some micro-damage began to appear inside the specimen, and some micro-cracks occurred. As loading continued, the third stage was reached. At this stage, acoustic emission signals increased significantly and the energy value increased significantly. Obvious cracks appeared inside the specimen, eventually losing resistance and causing damage.

In general, the F-T cycles had similar effects on the three groups of PAMs. That is, the first stage was gradually shortened, and the third stage gradually increased. The occurrence of the second stage gradually moved forward. Mixtures that experienced more F-T cycles began to damage at lower load levels. This shows that the freeze-thaw cycle had a significant adverse effect on PAMs, which made the mixtures more likely to cause early failure under the load.

Specifically, we determined the corresponding load levels when the first AE (acoustic emission) signal and the AE signal with the maximum energy value appeared, and these were calibrated by

the red dotted line. As shown in Figure 4, the load levels of the three groups of PAMs showed a decreasing trend when the first acoustic emission signal appeared. For example, for the PAM-18 group, the first acoustic emission event occurred at a load level of about 0.4 for the specimens without F-T cycles. However, for a test piece that had undergone 20 F-T cycles, the first acoustic emission event occurred when the load level was approximately 0.16; this shows that the F-T cycles advanced the micro-damage of the specimens. In addition, the test piece without F-T cycles had an acoustic emission event with maximum energy value when the load level was about 0.9; however, for the specimens that had undergone 20 F-T cycles, an acoustic emission event with a maximum energy value occurred when the load level was only about 0.75. This indicates that after the F-T cycles, the failure stage of specimens during the loading process was advanced. The other two PAMs showed the same pattern.

The difference was the maximum energy value of the acoustic emission signal of the three groups of PAMs under load. The average energy of PAM-18, PAM-21, and PAM-25 was 348.54, 561.48, and 1160.26 mv*μs, respectively. It can be seen that the larger the proportion of coarse aggregate, the greater the energy released by the PAM when the internal cracks of the specimen were generated.

3.2. Indirect Tensile and Compression Experiments at Normal Temperature

3.2.1. Indirect Tensile Test

The effects of F-T cycles on the performance of each group of PAMs were characterized by calculating the indirect tensile strength and failure strain. The specific experimental results are shown in Figure 5.

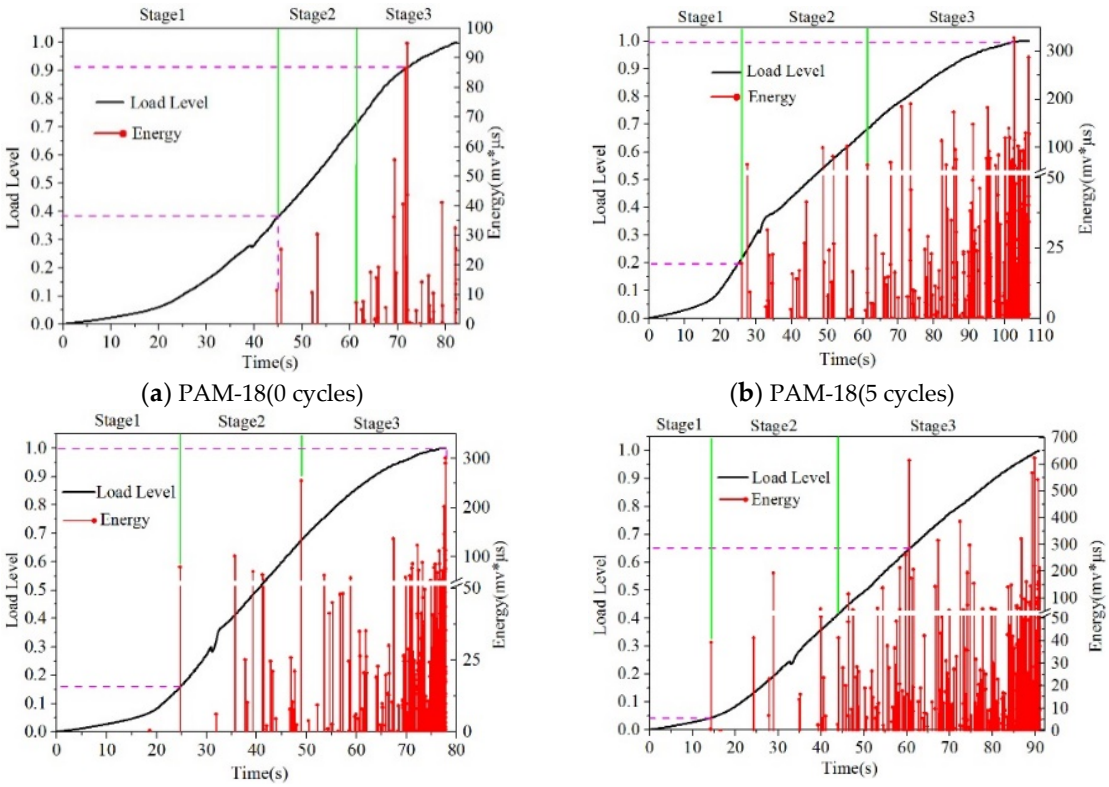

(**a**) PAM-18(0 cycles)

(**b**) PAM-18(5 cycles)

(**c**) PAM-18(10 cycles)

(**d**) PAM-18(15 cycles)

Figure 4. *Cont.*

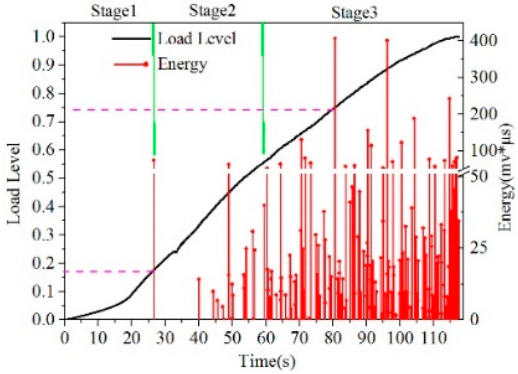

(**e**) PAM-18(20 cycles)

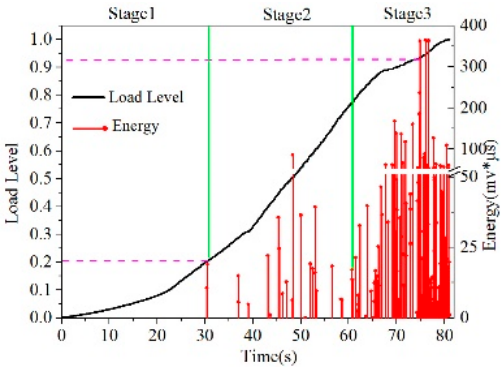

(**f**) PAM-21(0 cycles)

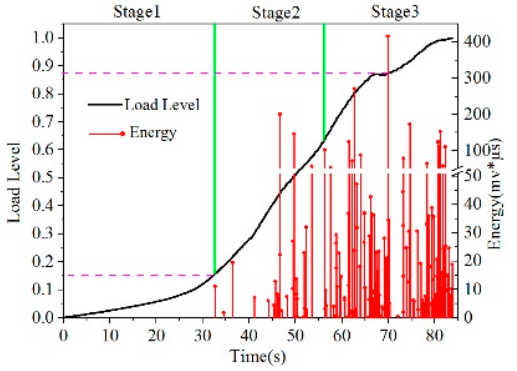

(**g**) PAM-21(5 cycles)

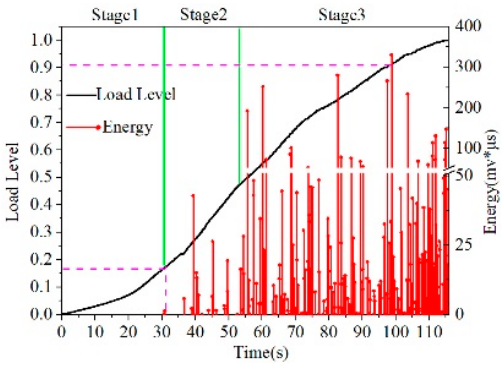

(**h**) PAM-21(10 cycles)

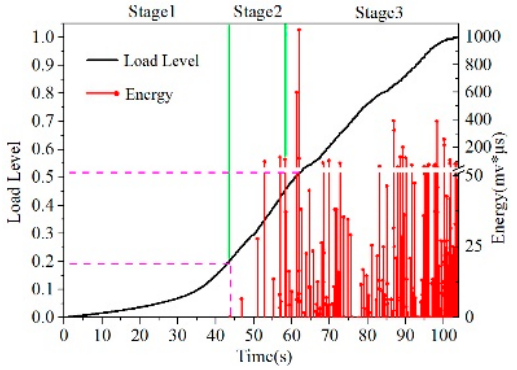

(**i**) PAM-21(15 cycles)

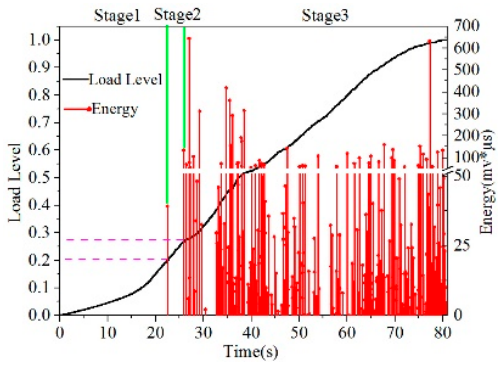

(**j**) PAM-21(20 cycles)

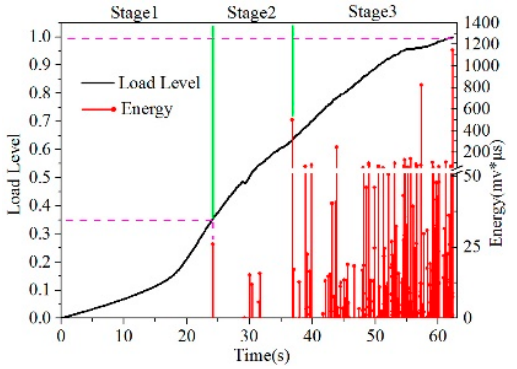

(**k**) PAM-25(0 cycles)

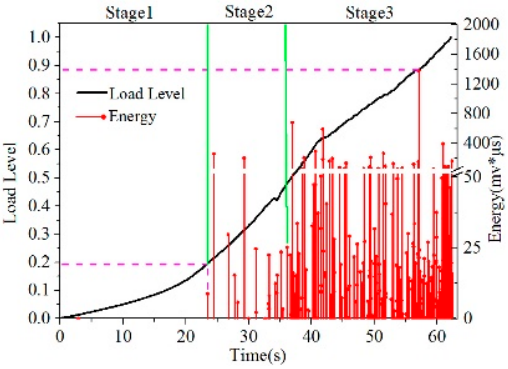

(**l**) PAM-25(5 cycles)

Figure 4. *Cont.*

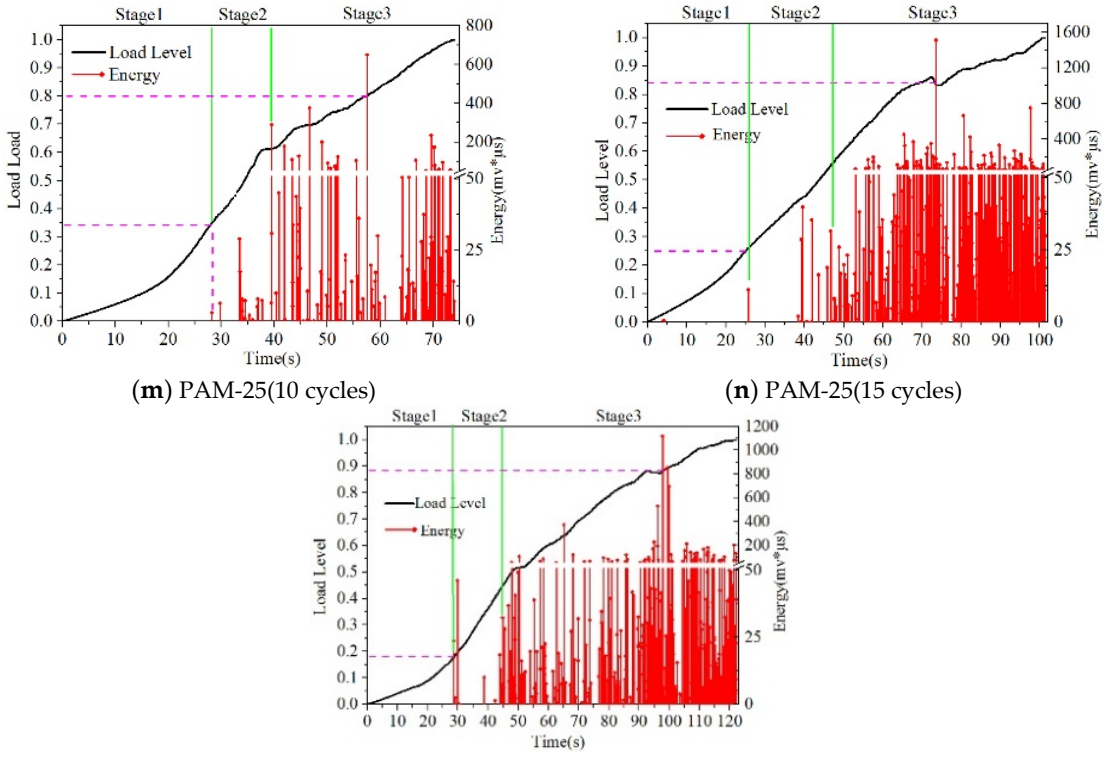

(**m**) PAM-25(10 cycles) (**n**) PAM-25(15 cycles)

(**o**) PAM-25(20 cycles)

Figure 4. Low-temperature splitting test results.

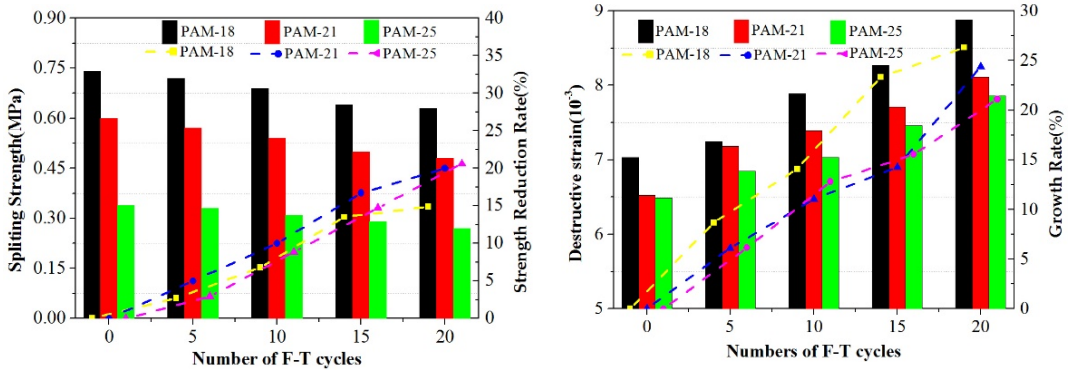

(**a**)The splitting strength (**b**)The destructive strain

Figure 5. Normal temperature indirect tensile test results.

In Figure 5a,b, the histogram shows the indirect tensile strength and failure strain respectively. Dotted lines indicate their change rates. First, as shown in Figure 5a, in general, the higher the air void, the smaller the strength of the PAM. In addition, the indirect tensile strength of the three groups of PAM decreased with the increase of the number of F-T cycles. When the number of F-T cycles reached 20, the strength of the PAM-18 decreased by 14.86%, while the PAM-21 and PAM-25 decreased by 20% and 20.59%, respectively. This shows that under the freeze-thaw cycle conditions in this study, from the perspective of indirect tensile strength, the PAM-18 group suffered less damage.

For failure strain, the larger the air void of the mixture, the smaller the failure strain, which shows that the larger the internal air void of PAM, the smaller its deformation ability is. Further, with the increase of the number of F-T cycles, the damage strain of the three PAMs gradually increased; e.g., the PAM-18 group reached a rate of 26.32% when the number of F-T cycles reached 20. This phenomenon

shows that although the larger the air void, the better the permeability of PAM, from the perspective of indirect tensile strength and failure strain, too large an air void will aggravate the adverse effect of freeze-thaw cycles on PAM.

3.2.2. Compression Test

As shown in Figure 6, compression strength and failure strain are used to represent the results of compression testing. Similar to the splitting test, the larger the air void is, the smaller the compressive strength of PAM is. In addition, with the increase of F-T cycles, the compressive strength of the three PAMs decreased gradually. Specifically, there was no significant difference in the reduction rate after the first 15 F-T cycles. Until the 20th freeze-thaw cycle, the strength reduction rate of the three groups of PAMs had a significant difference. It can be seen that in the air void range of 18–25%, the larger the air void, the greater the long-term freeze thaw effect on the mixture under compression.

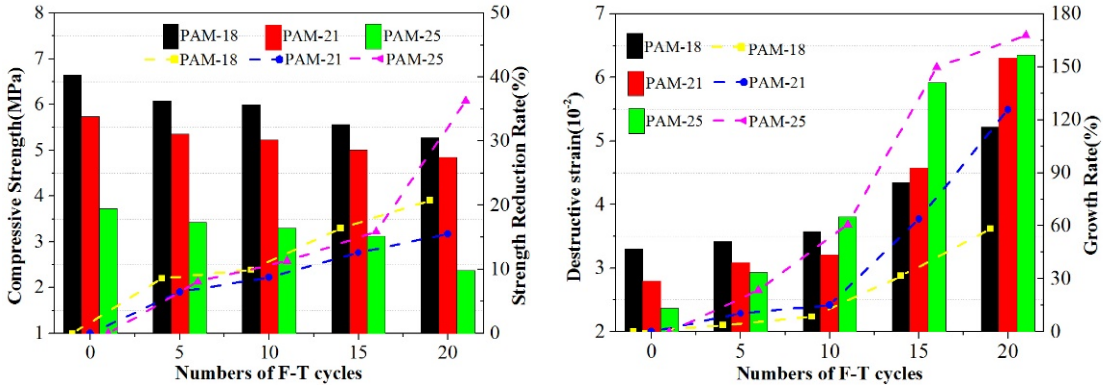

(**a**)The compressive strength (**b**)The destructive strain

Figure 6. Compression test results at normal temperature.

In addition, the failure strain of the three groups of PAMs increased with the number of F-T cycles. It can be seen from Figure 6b that under the effect of 0–5 F-T cycles, the growth rates of the compression failure strain of the three groups of PAMs are arranged in descending order of PAM-18, PAM-21, PAM-25. After 15 cycles, the increasing order of the growth rate of failure strain was PAM-25, PAM-21, PAM-18, which is different from the results of the splitting test. In the compression test, the PAM with larger air voids showed greater strain growth rate under the action of F-T cycles. This was due to different load application methods. When the specimens were compressed, there was a gradual compaction process. Under the F-T cycles, the larger the air void of the specimen, the greater the damage, which resulted in greater failure strain. This indicates that under compression load, the failure strain of larger air void PAMs was more sensitive to F-T cycles.

3.3. Cantabro Particle Loss Test

It can be seen from Figure 7 that the air void is a very important index affecting the spalling resistance of PAMs. For the specimens without F-T cycles, the Cantabro particle loss rate of the PAM-18 was only 3.01% and that of the PAM-21 was 6.92%, while for the PAM-25, the loss rate surged to 25.12%. It can be seen from this that when the air void was too large, the spalling resistance of the PAM decreased rapidly.

In addition, the F-T cycles had a great impact on the Cantabro particle loss rate of PAMs. With the increase of F-T cycles, the loss rate of the three mixtures increased gradually, and the larger the air void, the greater the adverse effect. Specifically, after 20 F-T cycles, the Cantabro particle loss rate for the PAM-18 increased from 3.01% to 4.97%. For the PAM-21, the loss rate increased from 6.92% to 11.17%; however, these two PAMs still meet the requirements of less than 15% in the specifications [25].

However, for the PAM-25, the loss rate increased from 25.12% to 54.41%. It can be seen that if the air void of PAM is too large, not only will the adhesion between the asphalt and aggregate be significantly reduced, but the adverse effect of the F-T cycles on the cohesion of asphalt and aggregate will be more obvious. Therefore, the air void of the PAM in seasonally frozen areas must not be too large.

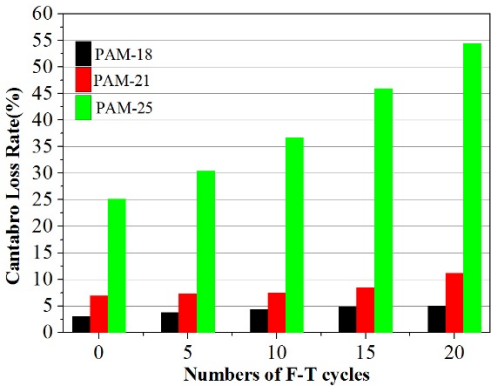

Figure 7. Cantabro particle loss test results.

3.4. Dynamic Creep Test Results

By comparing results shown in Figure 8a–c, it can be seen that the larger air void of the PAM, the larger the permanent deformation caused by the dynamic load. In addition, the F-T cycles had a greater impact on the high-temperature creep properties of these three mixtures.

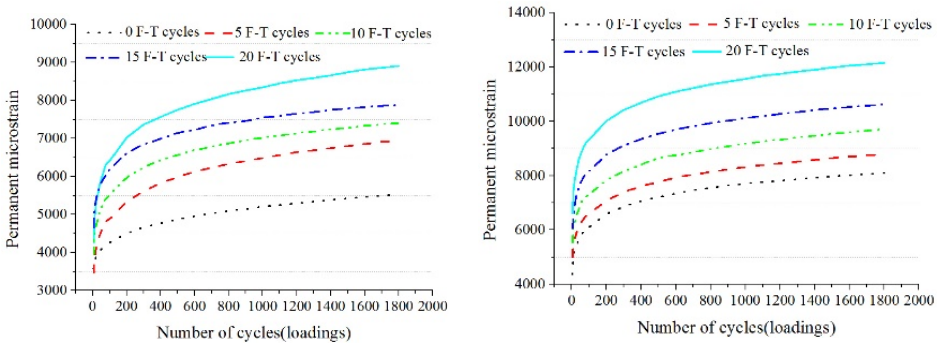

(**a**) PAM-18 (**b**) PAM-21

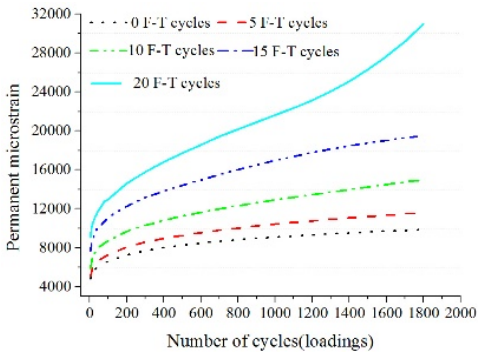

(**c**) PAM-25

Figure 8. Dynamic creep test results.

In order to further analyze the effect of F-T cycles on the high-temperature performance of the three groups of mixtures, creep strain slope and creep stiffness were used to characterize them, as shown in Figure 9. The larger the creep strain slope was, the easier the deformation was, and the larger the creep

stiffness was, the stronger the deformation resistance was. In general, the creep strain slope increased as the air void of the mixture increased. For example, for specimens subjected to 10 F-T cycles, the creep strain slope of PAM-18, PAM-21, and PAM-25 was 0.7, 0.93, and 2.98, respectively. Further, the creep strain slope of the three groups of PAMs increased with the number of F-T cycles. In particular, for the PAM-25 group, the creep strain slope increased dramatically after 20 F-T cycles. It can also be seen from the creep curve in Figure 8c that the third stage of the creep process obviously occurred, and the deformation of the test piece increased rapidly, and it can be considered that the test piece had creep failure. This shows that the larger the air void of PAM, the greater the adverse effect of F-T cycles was on its high-temperature creep performance. The creep stiffness index shows the same rule.

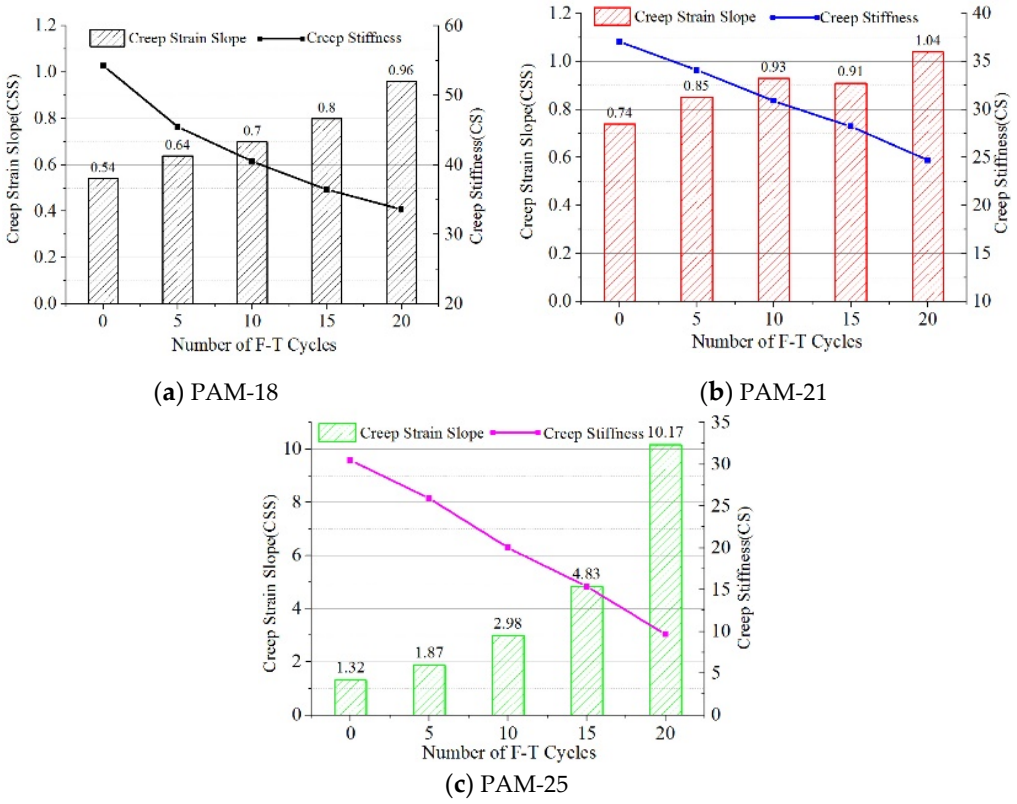

(**a**) PAM-18 (**b**) PAM-21

(**c**) PAM-25

Figure 9. Creep strain slope and creep stiffness of three PAMs.

4. Conclusions

In this paper, the influence of F-T cycles on the performance decay of porous asphalt mixtures with air voids of 18%, 21%, and 25% was studied by performing a low-temperature splitting test, a normal temperature splitting and compression test, a Cantabro particle loss test, and a dynamic creep test. Conclusions can be described as follows:

1. Acoustic emission parameters well reflect the stress characteristics of the specimens during the low-temperature splitting process. Under the effect of F-T cycles, the damage stage and destruction stage of the three groups of PAMs were advanced. The larger the proportion of coarse aggregate in the PAM, the greater the single energy released by the specimen during the destruction process.
2. The indirect tensile strength of PAM decreases rapidly with the increase of air void and the number of F-T cycles. In contrast, the failure strain increases with the increase of F-T cycles. PAM-18 was the least affected by the F-T cycles. The results of compression experiments at normal temperature showed similar rules.

3. The air void is the main factor that affects the cohesiveness between aggregate and asphalt. The larger the air void, the larger the Cantabro particle loss of the specimen, and the greater the adverse effect of the freeze-thaw cycle on the adhesion of the aggregate to the asphalt. When the air void reached 25%, the Cantabro particle loss rate of the specimen was far greater than the 15% in the specifications, regardless of whether it suffered the F-T cycles or not.
4. Both the air void and F-T cycles are important factors affecting the high-temperature viscoelastic properties of PAM. As the air void and the number of F-T cycles increased, the creep strain slope of the three groups of PAMs gradually increased and the creep stiffness gradually decreased. When the air void is greater than 21%, the adverse effects of F-T cycles become apparent.
5. For seasonal frozen regions that are often subjected to F-T cycles, the air void of PAM should be minimized while ensuring drainage performance. It is recommended to keep the air void to 21% or less to avoid early damage to the pavement.

Author Contributions: Conceptualization, C.C. and Y.-C.C.; methodology, C.C. and Y.Z.; validation, Y.C.; formal analysis, Y.Z.; investigation, C.C. and Y.Z.; writing—original draft preparation, C.C.; writing—review and editing, Y.C. and B.Z.; project administration, Y.-C.C. and Y.Z.; funding acquisition, Y.-C.C. All authors have read and agreed to the published version of the manuscript.

Funding: This research was funded by the Science Technology Development Program of Jilin Province, grant number 20180201026SF, the National Natural Science Foundation of China, grant number 51678271.

Acknowledgments: The authors would like to thank the anonymous reviewers for their constructive suggestions and comments to improve the quality of the paper. In addition, thanks to the Jilin Dongsheng company for the supply of raw materials.

Conflicts of Interest: The authors declare no conflict of interest.

References

1. Cobbinah, P.B.; Kosoe, E.A.; Diawuo, F. Environmental planning crisis in urban Ghana: Local responses to nature's call. *Sci. Total. Environ.* **2020**, *701*, 134898. [CrossRef] [PubMed]
2. Sun, Y.; Chen, S.S.; Lau, A.Y.T.; Tsang, D.C.W.; Mohanty, S.K.; Bhatnagar, A.; Rinklebe, J.; Lin, K.Y.A.; Ok, Y.S. Waste-derived compost and biochar amendments for stormwater treatment in bioretention column: Co-transport of metals and colloids. *J. Hazard. Mater.* **2020**, *383*, 121243. [CrossRef] [PubMed]
3. Ye, Q.; Han, Y.; Zhang, S.; Gao, Q.; Zhang, W.; Chen, H.; Gong, S.; Shi, S.Q.; Xia, C.; Li, J. Bioinspired and biomineralized magnesium oxychloride cement with enhanced compressive strength and water resistance. *J. Hazard. Mater.* **2020**, *383*, 121099. [CrossRef] [PubMed]
4. Sun, D.Q.; Sun, G.Q.; Zhu, X.Y.; Xiao, F.P.; Dai, Z.W.; Liu, F.L. Electrical characteristics of conductive ultrathin bonded wearing course for active deicing and snow melting. *Int. J. Pavement. Eng.* **2019**, *20*, 1299–1308. [CrossRef]
5. Jiang, L.; Wang, L.C.; Wang, S.Y. A novel solar reflective coating with functional gradient multilayer structure for cooling asphalt pavements. *Constr. Build. Mater.* **2019**, *210*, 13–21. [CrossRef]
6. Lu, G.Y.; Renken, L.; Li, T.S.; Wang, D.W.; Li, H.; Oeser, M. Experimental study on the polyurethane-bound pervious mixtures in the application of permeable pavements. *Constr. Build. Mater.* **2019**, *202*, 838–850. [CrossRef]
7. Tang, T.C.; Anupam, K.; Kasbergen, C.; Scarpas, A.; Erkens, S. A finite element study of rain intensity on skid resistance for permeable asphalt concrete mixes. *Constr. Build. Mater.* **2019**, *220*, 464–475. [CrossRef]
8. Liu, Z.M.; Luo, S.; Quan, X.; Wei, X.H.; Yang, X.; Li, Q. Laboratory evaluation of performance of porous ultra-thin overlay. *Constr. Build. Mater.* **2019**, *204*, 28–40. [CrossRef]
9. Khaki, A.M.; Forouhid, A.E.; Zare, M. Comparison of the noise level and the skid resistance of asphalt pavement mixtures on road surface. *J. Meas. Eng.* **2015**, *3*, 71–76.
10. Hu, K. Key Technology of Research of Efficient Separation of Construction & Demolition Waste in Pavement Engineering. Ph.D. Thesis, Chang'an University, Xi'an, China, 2017.
11. Zhang, L. Design and Performance of Experimental Research of Hot Recycled Asphalt Mixture. Master's Thesis, Chongqing Jiaotong University, Chongqing, China, 2014.

12. Zarrinkamar, B.T.; Modarres, A. Optimizing the asphalt pavement cold in-place recycling process containing waste pozzolans based on economic-environmental-technical criteria. *J. Clean. Prod.* **2020**, *242*, 11. [CrossRef]
13. Yan, K.Z.; Li, L.L.; Zheng, K.G.; Ge, D.D. Research on properties of bitumen mortar containing municipal solid waste incineration fly ash. *Constr. Build. Mater.* **2019**, *218*, 657–666. [CrossRef]
14. Cheng, Y.C.; Wang, W.S.; Tan, G.J.; Shi, C.L. Assessing High- and Low-Temperature Properties of Asphalt Pavements Incorporating Waste Oil Shale as an Alternative Material in Jilin Province, China. *Sustainability* **2018**, *10*, 2179. [CrossRef]
15. Liu, W.; Li, H.; Zhu, H.; Xu, P. Properties of a Steel Slag-Permeable Asphalt Mixture and the Reaction of the Steel Slag-Asphalt Interface. *Materials* **2019**, *12*, 3603. [CrossRef] [PubMed]
16. Wu, H.N.; Li, P.; Nian, T.F.; Zhang, G.H.; He, T.; Wei, X.Y. Evaluation of asphalt and asphalt mixtures' water stability method under multiple F-T cycles. *Constr. Build. Mater.* **2019**, *228*, 15. [CrossRef]
17. Guo, Q.L.; Li, G.Y.; Gao, Y.; Wang, K.Y.; Dong, Z.Z.; Liu, F.C.; Zhu, H. Experimental investigation on bonding property of asphalt-aggregate interface under the actions of salt immersion and F-T cycles. *Constr. Build. Mater.* **2019**, *206*, 590–599. [CrossRef]
18. Wang, W.S.; Cheng, Y.C.; Ma, G.R.; Tan, G.J.; Sun, X.; Yang, S.T. Further Investigation on Damage Model of Eco-Friendly Basalt Fiber Modified Asphalt Mixture under F-T cycles. *J. Appl. Sci.* **2019**, *9*, 60. [CrossRef]
19. TehSek, Y.; Meor, O.H. Asphalt mixture workability and effects of long-term conditioning methods on moisture damage susceptibility and performance of warm mix asphalt. *Constr. Build. Mater.* **2019**, *207*, 316–328.
20. Zhang, Q.L.; Huang, Z.Y. Investigation of the micro-characteristics of asphalt mastics under dry-wet and F-T cycles in a coastal salt environment. *Materials* **2019**, *12*, 2627. [CrossRef]
21. You, L.Y.; You, Z.P.; Dai, Q.L.; Xie, X.F.; Washko, S.; Gao, J.F. Investigation of adhesion and interface bond strength for pavements underlying chip-seal: Effect of asphalt-aggregate combinations and F-T cycles on chip-seal. *Constr. Build. Mater.* **2019**, *203*, 322–330. [CrossRef]
22. Nguyen, T.H.; Ahn, J.; Lee, J.; Kim, J.H. Dynamic Modulus of Porous Asphalt and the Effect of Moisture Conditioning. *Materials* **2019**, *12*, 1230. [CrossRef]
23. Ji, J.; Yao, H.; Yuan, Z.K.; Suo, Z.; Xu, Y.; Li, P.F.; You, Z.P. Moisture susceptibility of warm mix asphalt (WMA) with an organic wax additive based on X-ray computed tomography (CT) technology. *Adv. Mater. Sci. Eng.* **2019**, *2019*, 1–12. [CrossRef]
24. Badeli, S.; Carter, A.; Dore, G. Effect of laboratory compaction on the viscoelastic characteristics of an asphalt mix before and after rapid F-T cycles. *Cold. Reg. Sci. Technol.* **2018**, *146*, 98–109. [CrossRef]
25. Ministry of Housing and Urban-Rural Development of the People's Republic of China. *Technical Specification for Permeable Asphalt Pavement*; Ministry of Housing and Urban-Rural Development of the People's Republic of China: Beijing, China, 2012. (In Chinese)
26. Cheng, Y.C.; Chai, C.; Liang, C.Y.; Chen, Y. Mechanical performance of warm-mixed porous asphalt mixture with steel slag and crumb-rubber-SBS modified bitumen for seasonal frozen regions. *Materials* **2019**, *12*, 857. [CrossRef] [PubMed]
27. Cheng, Y.C.; Chai, C.; Zhang, Y.W.; Chen, Y.; Zhu, B. A new eco-friendly porous asphalt mixture modified by crumb rubber and basalt fiber. *Sustainability* **2019**, *11*, 5754. [CrossRef]
28. Ministry of Transport of the People's Republic of China. *Standard Test Methods of Bitumen and Bituminous Mixtures for Highway Engineering*; Ministry of Transport of the People's Republic of China: Beijing, China, 2011. (In Chinese)
29. Jiao, Y.B.; Liu, S.Q.; Fu, L.X.; Shan, W.C. Fracture monitoring of SBS and crumb rubber modified porous asphalt mixtures under compression and splitting testing using acoustic emission technique. *J. Mater. Civ. Eng.* **2019**, *31*, 12. [CrossRef]
30. Jiao, Y.B.; Fu, L.X.; Shan, W.C.; Liu, S.Q. Damage fracture characterization of pervious asphalt considering temperature effect based on acoustic emission parameters. *Eng. Fract. Mech.* **2019**, *210*, 147–159. [CrossRef]
31. The British Standards Institution. *BS EN 12697-25, Bituminous Mixtures—Test Methods for Hot Mix Asphalt Part 25: Cyclic Compression Test*; BSI Standard: London, UK, 2013.